ChemPubSoc Europe

DOI: 10.1002/cphc.201700896

CHEMPHYSCHEM Communications

Effect of Water Addition during Preparation on the Early-Time Photodynamics of $CH_3NH_3PbI_3$ Perovskite Layers

S. Aphrham,[a] Q. Pan,[a, c] S. F. Zaccarine,[a] K. M. Felter,[b] J. Thieme,[b] K. J. H. van den Nieuwenhuijzen,[a] J. E. ten Elshof,[a] and A. Huijser*[a]

The effect of water addition during preparation of a $CH_3NH_3PbI_3$ layer on the photodynamics is studied by femtosecond transient absorption. Both the regular perovskite and the aqueous analogue show charge thermalisation on a timescale of about 500 fs. This process is, however, less pronounced in the latter layer. The spectral feature associated with hot charges does not fully decay on this timescale, but also shows a long-lived (sub-ns) component. As water molecules may interfere with the hydrogen bonding between the $CH_3NH_3^+$ cations and the inorganic cage, this effect is possibly caused by immobilisation of cation motion, suggesting a key role of $CH_3NH_3^+$ dipole reorientation in charge thermalisation. This effect shows the possibility of controlling hot charge carrier cooling to overcome the Shockley–Queisser limit.

Hybrid perovskites are attracting tremendous attention as highly promising materials for low-cost and efficient photovoltaics,[1] light-emitting diodes,[2] memory devices[3] and nonlinear optical devices.[4] These fascinating materials, generally based on an ABX_3 crystal structure where A represents an organic cation embedded in an inorganic cage of B (lead or tin) and a halogen X, combine the solution processability of molecular materials with the low exciton binding energy,[5] high charge mobility and long diffusion length[6] of inorganic semiconductors. Soon after Miyasaka's publication on a perovskite dye-sensitised solar cell in 2009,[7] the power conversion efficiency realised increased in an exponential manner to 22.1% recently.[8]

As this technology is very young and research has predominantly focused on the development of materials and devices, insight into the photophysical dynamics enabling this impressive performance is still developing. The most commonly used $CH_3NH_3PbI_3$ material has a broad absorption spectrum with maxima around 480 nm and 760 nm. The origin of this dual behaviour is under debate and generally explained in terms of filling of valence/conduction bands,[9] multiple valence and conduction bands[6c, 10] and distinct charge transfer transitions.[11] Recent quantum chemical calculations indicate that the valence band upper states have a strong contribution from iodide, whereas the bottom of the conduction band is possibly formed of molecular orbitals dominated by Pb states.[12] The $CH_3NH_3^+$ cation likely gives rise to energy levels above the conduction band edge. Photoexcitation in the red has been proposed to mainly give $I^- \rightarrow Pb^{2+}$ charge transfer, while excess photoexcitation energy may also lead to $I^- \rightarrow CH_3NH_3^+$ charge transfer and potentially even to movement of the I^- ion.[13]

An intriguing phenomenon is the rotation of the organic cation.[14] Its role in the photophysical properties of hybrid perovskites has been studied using a variety of theoretical approaches and spectroscopic techniques.[15] Hybrid perovskites have been demonstrated to show an optical Stark effect[13a, 16] due to photoinduced generation of charge carriers and possibly also due to a response of $CH_3NH_3^+$ dipole orientations. The energy landscape for motion and the energetically most stable orientation of an ensemble of $CH_3NH_3^+$ dipoles is under debate.[17] Neutron scattering experiments have shown a $\approx$14 ps reorientation time of the $CH_3NH_3^+$ cation,[18] while ultrafast 2D vibrational spectroscopy experiments have demonstrated a $\approx$300 fs "wobbling-in-a-cone" motion and a $\approx$3 ps jump-like reorientation relative to the inorganic cage.[19] These dipole motions may well be essential for the unique properties of hybrid perovskites and their role in exciton dissociation, charge cooling, separation and recombination is intensely debated.[15, 17d, 20] The long charge carrier lifetime has been explained by a dipole-induced stabilisation effect resulting in the formation of large polarons.[21] DFT calculations have demonstrated an important role of ferroelectric domain walls in charge separation.[22] Monte Carlo simulations have shown that collective rotation of $CH_3NH_3^+$ dipoles supports separation of electrons and holes into spatially distinct nanodomains following different current pathways, suppressing charge carrier recombination.[23] Another recent theoretical work has reported on a deformation of the inorganic cage induced by rotation of $CH_3NH_3^+$ cations, resulting in separation of photoinduced electrons and holes into spatially separated charge carrier stripes.[24] Also a variety in dynamic hydrogen bonding interac-

[a] S. Aphrham, Dr. Q. Pan, S. F. Zaccarine, K. J. H. van den Nieuwenhuijzen, Prof. Dr. J. E. ten Elshof, Dr. A. Huijser
MESA+ Institute for Nanotechnology
University of Twente
7500 AE Enschede (The Netherlands)
E-mail: j.m.huijser@utwente.nl

[b] K. M. Felter, J. Thieme
Chemical Engineering department
Faculty of Applied Sciences
Delft University of Technology
2600 GA Delft (The Netherlands)

[c] Dr. Q. Pan
Present address: Institute of Molecules and Materials
Radboud University Nijmegen
6525 AJ Nijmegen (The Netherlands)

Supporting Information for this article can be found under: https://doi.org/10.1002/cphc.201700896.

tions between the NH_3^+ group of the cation and the I^- ions of the inorganic cage[19b,25] may well be important.

The performance of $CH_3NH_3PbI_3$ based solar cells is well known to depend on the preparation.[26] The microstructure has been observed to have a pronounced effect on trap states, electron-hole interactions and charge carrier lifetimes.[27] The effects of water on the photovoltaic performance have recently become a topic of interest within the perovskite community, although results are sometimes contrasting. The presence of water has both been observed to accelerate degradation[28] and also improve the device performance and stability.[29] The perovskite crystal size, charge carrier lifetime and solar cell efficiency have been found to increase with water content for additions up to 5 vol% H_2O to the solutions used for layer preparation.[30] Both reversible and irreversible effects of water have been observed.[31] Water molecules have also been observed to interfere with the hydrogen bonding interactions between the $CH_3NH_3^+$ cation and the inorganic cage.[32] The present work therefore focuses at the role of hydration in the early-time photodynamics, and highlights its significant role in the hot charge carrier lifetime.

The UV/Vis absorption spectra shown in Figure 1, of layers of regular $CH_3NH_3PbI_3$ prepared following a two-step spin-coating procedure (see Experimental Section) and $CH_3NH_3PbI_3$ prepared from solutions containing 1 vol% H_2O are nearly similar and both show maxima at about 760 and 480 nm, in agreement with earlier studies.[33] Also, the structural analysis data (provided in the Supporting Information, Section 1) are nearly similar. The X-ray diffraction patterns indicate the presence of both $CH_3NH_3PbI_3$ and PbI_2 in the layer, in agreement with earlier studies using a similar preparation procedure.[34] The amount of PbI_2 in the aqueous layer may be slightly higher. The observed difference with the regular layer is though comparable to variations between samples, which may be due to small fluctuations in annealing temperature. The infrared reflectance spectra of both perovskite layers are also rather similar. The signal around ca. 3500 cm^{-1} indicative of intercalated H_2O is weak relative to earlier observations for layers exposed to humid air,[32b] indicating that addition of 1 vol% H_2O to the solutions used for preparation only leads to a low degree of water intercalation. The scanning electron micrographs show a homogeneous nanomorphology for both layers, with a typical crystal size of about 50 nm. The $CH_3NH_3PbI_3$ layer prepared from solutions containing 1 vol% H_2O shows additional features with a size of a few nm.

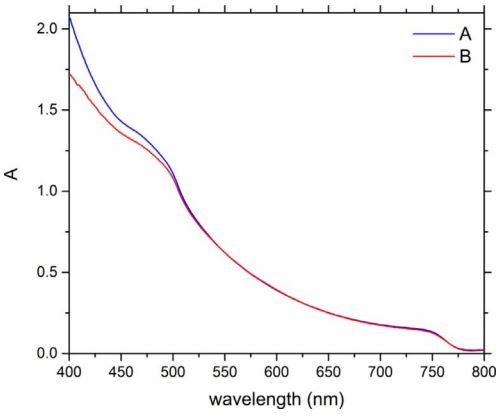

Figure 1. UV/Vis absorption spectra of layers of: A) $CH_3NH_3PbI_3$ and B) $CH_3NH_3PbI_3$ prepared from solutions containing 1 vol% H_2O.

The impact of water addition on the charge carrier dynamics was studied by femtosecond transient absorption spectroscopy. Figure 2A shows the transient absorption spectra of the $CH_3NH_3PbI_3$ layer at 525 nm photoexcitation for various time delays between pump and probe. The two absorption bands in the visible around 480 and 760 nm shown in Figure 1 give rise to two negative ground state bleach (GSB) signals. The photogenerated hot charge carriers give rise to a short-lived excited state absorption (ESA) band around 780 nm.[35] The intensity of this ESA band decreases on lowering the excess photoexcitation energy, as evident from comparison with the transient absorption data at 700 nm photoexcitation (see Supporting Information, section 2). The broad ESA in the visible is generally attributed to charge carriers.[16b] Figure 2B shows the kinetic traces at key wavelengths. The ESA around 780 nm decays at a sub-ps time scale indicative of charge cooling.[35b] This band extends into the infrared, as evident from the sub-ps decay component in the kinetic trace at 840 nm. The long-lived (sub-ns) component in this signal is likely due to ESA by charge carriers. The lowest energy GSB band (with a maximum around 745 nm) builds up within the instrumental response time and further develops on a sub-ps time scale, likely also

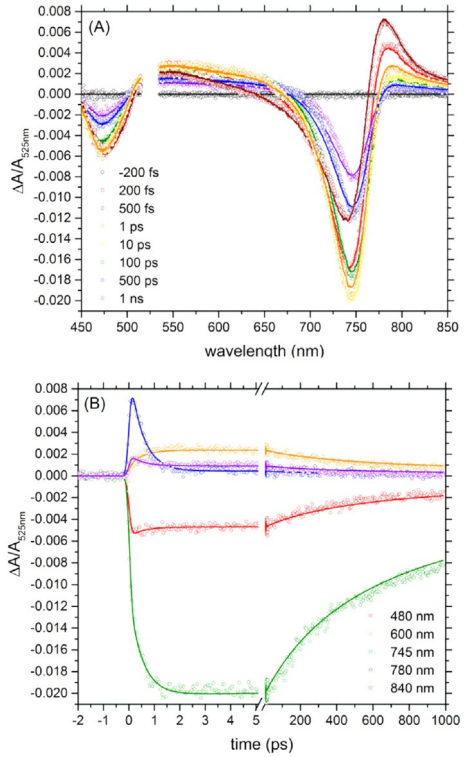

Figure 2. A) Transient absorption spectra at 525 nm photoexcitation and B) kinetic traces of a $CH_3NH_3PbI_3$ layer. The solid lines present the fit to a sequential model where ultrafast (511 ± 2 fs) charge cooling is followed by second-order charge recombination occurring at a rate constant of $8 \pm 3 \times 10^{-10}$ $cm^3 s^{-1}$.

due to charge carrier cooling.[6c] The GSB signal also shows a redshift and narrowing in time, which effect is discussed below. The kinetic trace at 600 nm representative of the broad ESA band in the visible develops on a sub-ps time scale correlated to the decay in ≈780 nm ESA signal and ingrowth in GSB around 745 nm due to charge carrier cooling.[35b] The broad ESA band in the visible is likely overlapping with the second GSB signal around 480 nm, causing this GSB signal to become less negative on a sub-ps time scale after formation of the initial GSB within the instrumental response time. All transient absorption signals decay at a sub-ns time scale indicating charge carrier recombination. A photophysical model has been established through global and target analysis of the data (fit included as solid lines in Figure 2), in which charge carrier cooling occurring at a time constant of 511 ± 2 fs is followed by second-order charge recombination[9] with a rate constant of $8 \pm 3 \times 10^{-10}$ $cm^3 s^{-1}$.

Figure 3 A shows the transient absorption spectra at 525 nm photoexcitation of the $CH_3NH_3PbI_3$ layer prepared from solutions containing 1 vol% H_2O. Comparison with Figure 2 A shows a number of notable differences in spectrotemporal behaviour with the regular $CH_3NH_3PbI_3$ layer. The GSB signal around 480 nm relative to the 760 nm GSB is more intense. As the $CH_3NH_3^+$ cation is likely involved in the first electronic transition,[13] this effect may be caused by the proximity of a H_2O molecule to the cation. Also the transient absorption signal intensities have decreased. Another important difference involves the ESA around 775 nm. Though part of this signal decays on a sub-ps time scale similar to regular $CH_3NH_3PbI_3$, a longer-lived signal remains. This effect is also evident in the kinetic traces presented in Figure 3 B. All transient absorption signals decay at a sub-ns time scale indicating charge recombination. Fitting a similar sequential model used above gives a charge cooling time of 512 ± 3 fs and a second-order charge recombination rate of $1.0 \pm 0.5 \times 10^{-9}$ $cm^3 s^{-1}$. Evidently, the charge recombination dynamics are unaffected by the addition of 1 vol% H_2O to the solutions used for perovskite layer preparation. Note that the presence of PbI_2 in perovskite layers could slow down charge carrier recombination.[35c] The similar recombination dynamics observed for the regular and aqueous perovskite layers indicate a negligible impact of the possibly slightly higher amount of PbI_2 in the aqueous layer.

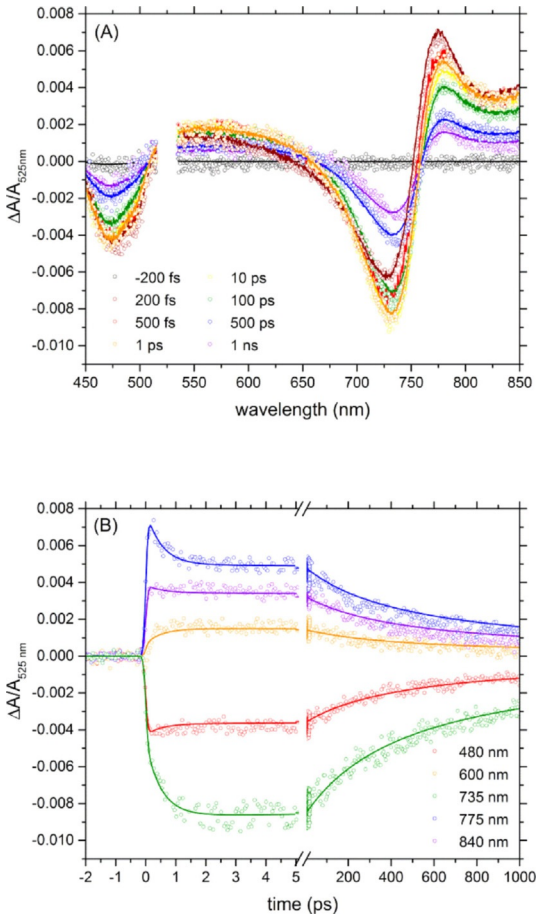

Figure 3. A) Transient absorption spectra at 525 nm photoexcitation and B) kinetic traces of a $CH_3NH_3PbI_3$ layer prepared from solutions containing 1 vol% H_2O. The solid lines present the fit to a sequential model where ultrafast (512 ± 3 fs) charge cooling is followed by second-order charge recombination occurring at a rate constant of $1.0 \pm 0.5 \times 10^{-9}$ $cm^3 s^{-1}$.

Figure 4 shows the normalised species associated spectra (SAS) obtained from the data analysis described above for both the regular $CH_3NH_3PbI_3$ layer and the layer prepared from solutions containing 1 vol% H_2O. SAS 1 represents the spectrum prior to charge carrier cooling, while SAS 2 applies to after thermalisation. For both layers the lowest energy GSB shows a redshift in time and also becomes narrower, which can be assigned to charge carrier cooling reducing the transient optical Stark effect induced by hot carriers.[35] The photoinduced change in local electric field responsible for the optical Stark effect observed may well be screened by rearrangement of $CH_3NH_3^+$ dipoles[13a] and also alter in time due to a change in electron-hole separation distance and concentration.[16b] Both SAS 1 and SAS 2 of the aqueous analogue show a ca. 10 nm blue shift relative to the spectra of the regular $CH_3NH_3PbI_3$ layer. This trend is in agreement with the observed widening in band gap induced by water intercalation.[36] However, the absence of a blue shift for the aqueous analogue relative to the regular perovskite at 700 nm photoexcitation (see Supporting Information, section 2) shows the need for excess

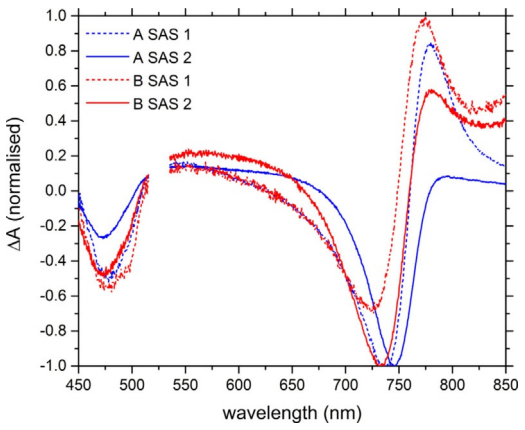

Figure 4. Normalised species associated spectra for layers of: A) $CH_3NH_3PbI_3$ and B) $CH_3NH_3PbI_3$ prepared from solutions containing 1 vol% H_2O.

photoexcitation energy, suggesting a difference in local electric field to be responsible for the blue shift.

A second important effect of H_2O addition is the temporal evolution of the ESA signal around 780 nm, indicative of hot charge carriers. The regular $CH_3NH_3PbI_3$ layer shows this feature only in SAS 1 representing early (sub-ps) time scales. On the contrary, the aqueous analogue shows this absorption band also in SAS 2, although less intense. This effect is also illustrated by the difference in the kinetic traces associated with hot charge carriers (blue traces in Figures 2B and Figures 3B). Although also for the hydrated analogue part of this signal decays on a sub-ps time scale, a longer-lived signal remains, indicating that less hot charge carriers are thermalised in the initial ultrafast (ca. 500 fs) cooling process.

As H_2O has been observed to interfere with the hydrogen bonding interactions between the $CH_3NH_3^+$ cation and the inorganic cage,[32b] this difference suggests a role of (possibly collective) $CH_3NH_3^+$ dipole reorientation in charge cooling. The presence of a H_2O molecule in the vicinity of a $CH_3NH_3^+$ cation is likely to slow down its motions. The combination of a ca. 500 fs decay component alike the regular perovskite layer combined with a long-lived component may be assigned to the coexistence of both single $CH_3NH_3^+$ cations and combinations of one $CH_3NH_3^+$ cation and one (or more) H_2O molecule(s) in the inorganic cage. As a result, a fraction of the $CH_3NH_3^+$ dipoles may be immobilised alike mixed halide perovskites,[19b] preserving a significant fraction of hot charge carriers till time scales exceeding 100 ps instead of thermalising within 1 ps. This partial immobilisation may play a role in the blue shifts observed (Figure 4), suggesting less screening of the photoinduced transient optical Stark effect. Also the effect of water addition on the nanomorphology discussed above may play a role in the observed slow charge carrier thermalisation.

Harvesting hot charge carriers offers the opportunity to overcome the Shockley–Queisser limit restricting the power conversion efficiency of photovoltaic devices. Layers of colloidal $CH_3NH_3PbBr_3$ perovskite nanocrystals have recently been demonstrated to show slow charge carrier cooling, which allowed extraction of hot carriers with an efficiency up to 83%.[37] The present work presents an alternative approach based on water addition, which may immobilise a fraction of the $CH_3NH_3^+$ cations in the perovskite, and possibly reduce the number of phonons available for charge carrier thermalisation. It can be anticipated that a similar effect may also be present in non-aqueous immobilised hybrid perovskites. Providing the device stability can be preserved, the observation of similar charge recombination dynamics for the aqueous analogue and the regular layer shows promise for introduction of this approach to control hot charge carrier cooling in solar cells.

Experimental Section

$CH_3NH_3PbI_3$ layers were prepared from PbI_2 (Sigma–Aldrich, 99.999%) and CH_3NH_3I by spincoating and annealing as described in previous work.[34] CH_3NH_3I was synthesised and purified as reported earlier[19a] and dried in a vacuum oven at 60 °C for 24 hours. The quartz and glass substrates used for perovskite layer deposition and sealing were plasma cleaned and dried in advance. Briefly, 50 μl of a precursor solution was deposited on the substrate while spinning it at 6500 rpm. This solution consisting of 1.3 M PbI_2 and 0.31 M CH_3NH_3I in 9:1 (v/v) *N*,*N*-dimethylformamide (Sigma–Aldrich, anhydrous, 99.8%) and dimethyl sulfoxide (Sigma–Aldrich, anhydrous, ≥99.9%) was prepared 24 hours in advance and filtered twice using a 0.2 μm pore size filter. After 13 seconds, the rate was reduced to 4000 rpm in 1 second, and after 5 seconds 75 μl of CH_3NH_3I solution in 2-propanol (0.063 M, Sigma–Aldrich, anhydrous, 99.5%) was deposited onto the precursor layer, followed by 39 seconds of spinning. After spincoating, the sample was annealed on a hotplate at 100 °C for 15 minutes, covered by a second quartz or glass substrate and sealed.

UV/Vis absorption spectra were recorded using a Shimadzu UV-1800 spectrophotometer. X-ray diffraction data were recorded on a Bruker D2 Phaser diffractometer. Scanning electron micrographs were recorded using a Zeiss Merlin high-resolution scanning electron microscope. IR reflectance spectra were recorded using a Bruker Vertex 70 FTIR spectrometer.

The femtosecond transient absorption system consists of an amplified Yb:KGW laser system (Light Conversion Pharos), which produces 1028 nm laser pulses at 5 kHz repetition rate. Part of this 1028 nm output was directed into an optical parametric amplifier (Light Conversion) to generate the 525 nm pump beam. The remaining part of the fundamental 1028 nm beam was guided through a delay stage and focused onto a CaF_2 crystal to generate a broadband white light continuum probe. The CaF_2 crystal was mounted on a continuously moving stage to avoid thermal damage. The polarisation angle between the pump and probe beams was set at magic angle (54.7°). The pulse energy of the 525 nm pump beam (diameter ca. 250 μm) was about 4×10^{13} photons cm^{-2}. The probe light transmitted by the perovskite sample was detected using a Helios detector (Ultrafast Systems). The differential absorbance probe signal between pump on and off was obtained by chopping the 525 nm pump beam at 2.5 kHz.

The transient absorption data were numerically corrected for chirp by fitting the onset of the kinetic traces at various probe wavelengths with a polynomial function, and subsequent correction of the time axis on basis of that polynomial function. From the ingrowth of the signals, the time resolution was estimated to be 100–150 fs. The open-source program Glotaran[38] was used for analysis of the data from −2 ps till 5 ps, while the data from 5 ps till 1 ns were analysed using Origin assuming second-order charge carrier recombination [Eq. (1)]:[9]

$$\frac{n_0}{n_t} - 1 = kn_0t \qquad (1)$$

The parameter n_0 represents the initial charge carrier density ($n_0 = j\alpha$, with j the pump fluency and α the absorption coefficient at the pump wavelength), k is the second-order rate constant for recombination and n_t is the charge carrier density in time t.

Acknowledgements

This work is supported by the Dutch Sectorplan for Physics and Chemistry. Bianca Ruel (Biomolecular Nanotechnology group, University of Twente) is acknowledged for help with sample char-

acterisation and Mark Smithers (Nanolab, University of Twente) for recording the scanning electron micrographs.

Keywords: cation immobilisation · hybrid perovskites · photodynamics · transient absorption · water addition

[1] a) M. A. Green, A. Ho-Baillie, H. J. Snaith, *Nat. Photonics* **2014**, *8*, 506 – 514; b) P. Gao, M. Gratzel, M. K. Nazeeruddin, *Energy Environ. Sci.* **2014**, *7*, 2448 – 2463; c) J. Burschka, N. Pellet, S. J. Moon, R. Humphry-Baker, P. Gao, M. K. Nazeeruddin, M. Gratzel, *Nature* **2013**, *499*, 316 – 319.

[2] Z. K. Tan, R. S. Moghaddam, M. L. Lai, P. Docampo, R. Higler, F. Deschler, M. Price, A. Sadhanala, L. M. Pazos, D. Credgington, F. Hanusch, T. Bein, H. J. Snaith, R. H. Friend, *Nat. Nanotechnol.* **2014**, *9*, 687 – 692.

[3] C. Gu, J. S. Lee, *Acs Nano* **2016**, *10*, 5413 – 5418; b) B. Hwang, J. S. Lee, *Sci. Rep.* **2017**, *7*, 673.

[4] B. S. Kalanoor, L. Gouda, R. Gottesman, S. Tirosh, E. Haltzi, A. Zaban, Y. R. Tischler, *Acs Photonics* **2016**, *3*, 361 – 370.

[5] A. Miyata, A. Mitioglu, P. Plochocka, O. Portugall, J. T. W. Wang, S. D. Stranks, H. J. Snaith, R. J. Nicholas, *Nature Phys.* **2015**, *11*, 582 – U594.

[6] a) C. Wehrenfennig, G. E. Eperon, M. B. Johnston, H. J. Snaith, L. M. Herz, *Adv. Mater.* **2014**, *26*, 1584 – 1589; b) S. D. Stranks, G. E. Eperon, G. Grancini, C. Menelaou, M. J. P. Alcocer, T. Leijtens, L. M. Herz, A. Petrozza, H. J. Snaith, *Science* **2013**, *342*, 341 – 344; c) G. C. Xing, N. Mathews, S. Y. Sun, S. S. Lim, Y. M. Lam, M. Gratzel, S. Mhaisalkar, T. C. Sum, *Science* **2013**, *342*, 344 – 347; d) C. S. Ponseca, T. J. Savenije, M. Abdellah, K. B. Zheng, A. Yartsev, T. Pascher, T. Harlang, P. Chabera, T. Pullerits, A. Stepanov, J. P. Wolf, V. Sundstrom, *J. Am. Chem. Soc.* **2014**, *136*, 5189 – 5192.

[7] A. Kojima, K. Teshima, Y. Shirai, T. Miyasaka, *J. Am. Chem. Soc.* **2009**, *131*, 6050 – 6051.

[8] NREL, https://www.nrel.gov/pv/assets/images/efficiency-chart.png.

[9] J. S. Manser, P. V. Kamat, *Nat. Photonics* **2014**, *8*, 737 – 743.

[10] B. Anand, S. Sampat, E. O. Danilov, W. N. Peng, S. M. Rupich, Y. J. Chabal, Y. N. Gartstein, A. V. Malko, *Phys. Rev. B* **2016**, *93*, 161205.

[11] K. G. Stamplecoskie, J. S. Manser, P. V. Kamat, *Energy Environ. Sci.* **2015**, *8*, 208 – 215.

[12] T. Hakamata, K. Shimamura, F. Shimojo, R. K. Kalia, A. Nakano, P. Vashishta, *Sci. Rep.* **2016**, *6*, 19599.

[13] a) M. Pazoki, T. J. Jacobsson, J. Kullgren, E. M. J. Johansson, A. Hagfeldt, G. Boschloo, T. Edvinsson, *Acs Nano* **2017**, *11*, 2823 – 2834; b) E. Mosconi, F. De Angelis, *ACS Energy Lett.* **2016**, *1*, 182 – 188.

[14] a) A. Poglitsch, D. Weber, *J. Chem. Phys.* **1987**, *87*, 6373 – 6378; b) T. Chen, B. J. Foley, B. Ipek, M. Tyagi, J. R. D. Copley, C. M. Brown, J. J. Choi, S. H. Lee, *Phys. Chem. Chem. Phys.* **2015**, *17*, 31278 – 31286.

[15] C. S. Ponseca, Y. X. Tian, V. Sundström, L. G. Scheblykin, *Nanotechnology* **2016**, *27*, 082001.

[16] a) Y. Yang, M. J. Yang, K. Zhu, J. C. Johnson, J. J. Berry, J. van de Lagemaat, M. C. Beard, *Nat. Commun.* **2016**, *7*, 12613; b) A. A. Paraecattil, J. De Jonghe-Risse, V. Pranculis, J. Teuscher, J. E. Moser, *J. Phys. Chem. C* **2016**, *120*, 19595 – 19602.

[17] a) Y. F. Chen, Y. T. Tsai, D. M. Bassani, L. Hirsch, *Appl. Phys. Lett.* **2016**, *109*, 213504; b) J. Jankowska, O. V. Prezhdo, *J. Phys. Chem. Lett.* **2017**, *8*, 812 – 818; c) J. S. Bechtel, R. Seshadri, A. Van der Ven, *J. Phys. Chem. C* **2016**, *120*, 12403 – 12410; d) J. Even, L. Pedesseau, C. Katan, *J. Phys. Chem. C* **2014**, *118*, 11566 – 11572.

[18] A. M. A. Leguy, J. M. Frost, A. P. McMahon, V. G. Sakai, W. Kochelmann, C. H. Law, X. E. Li, F. Foglia, A. Walsh, B. C. O'Regan, J. Nelson, J. T. Cabral, P. R. F. Barnes, *Nat. Commun.* **2015**, *6*, 7124.

[19] a) A. A. Bakulin, O. Selig, H. J. Bakker, Y. L. A. Rezus, C. Muller, T. Glaser, R. Lovrincic, Z. H. Sun, Z. Y. Chen, A. Walsh, J. M. Frost, T. L. C. Jansen, *J. Phys. Chem. Lett.* **2015**, *6*, 3663 – 3669; b) O. Selig, A. Sadhanala, C. Muller, R. Lovrincic, Z. Chen, Y. L. A. Rezus, J. M. Frost, T. L. C. Jansen, A. A. Bakulin, *J. Am. Chem. Soc.* **2017**, *139*, 4068 – 4074.

[20] a) C. Quarti, E. Mosconi, F. De Angelis, *Chem. Mater.* **2014**, *26*, 6557 – 6569; b) A. J. Neukirch, W. Y. Nie, J. C. Blancon, K. Appavoo, H. Tsai, M. Y. Sfeir, C. Katan, L. Pedesseau, J. Even, J. J. Crochet, G. Gupta, A. D. Mohite, S. Tretiak, *Nano Lett.* **2016**, *16*, 3809 – 3816.

[21] X. Y. Zhu, V. Podzorov, *J. Phys. Chem. Lett.* **2015**, *6*, 4758 – 4761.

[22] S. Liu, F. Zheng, N. Z. Koocher, H. Takenaka, F. Wang, A. M. Rappe, *J. Phys. Chem. Lett.* **2015**, *6*, 693 – 699.

[23] A. Pecchia, D. Gentilini, D. Rossi, M. Auf der Maur, A. Di Carlo, *Nano Lett.* **2016**, *16*, 988 – 992.

[24] X. Zhang, M. L. Zhang, G. Lu, *J. Phys. Chem. C* **2016**, *120*, 23969 – 23975.

[25] J. H. Lee, J. H. Lee, E. H. Kong, H. M. Jang, *Sci. Rep.* **2016**, *6*, 21687.

[26] a) J. J. Shi, H. Y. Wei, S. T. Lv, X. Xu, H. J. Wu, Y. H. Luo, D. M. Li, Q. B. Meng, *ChemPhysChem* **2015**, *16*, 842 – 847; b) L. L. Wang, W. C. Lin, C. McCleese, A. Kovalsky, Y. X. Zhao, C. Burda, *ChemPhysChem* **2017**, *18*, 47 – 50; c) A. Dualeh, N. Tetreault, T. Moehl, P. Gao, M. K. Nazeeruddin, M. Gratzel, *Adv. Funct. Mater.* **2014**, *24*, 3250 – 3258.

[27] a) G. Grancini, A. R. S. Kandada, J. M. Frost, A. J. Barker, M. De Bastiani, M. Gandini, S. Marras, G. Lanzani, A. Walsh, A. Petrozza, *Nat. Photonics* **2015**, *9*, 695 – 701; b) D. W. de Quilettes, S. M. Vorpahl, S. D. Stranks, H. Nagaoka, G. E. Eperon, M. E. Ziffer, H. J. Snaith, D. S. Ginger, *Science* **2015**, *348*, 683 – 686; c) Y. Wang, H. Y. Wang, M. Yu, L. M. Fu, Y. J. Qin, J. P. Zhang, X. C. Ai, *ChemPhysChem* **2017**, *18*, 310 – 317.

[28] a) J. L. Yang, B. D. Siempelkamp, D. Y. Liu, T. L. Kelly, *Acs Nano* **2015**, *9*, 1955 – 1963; b) R. Ruess, F. Benfer, F. Bocher, M. Stumpp, D. Schlettwein, *ChemPhysChem* **2016**, *17*, 1505 – 1511.

[29] a) X. Gong, M. Li, X. B. Shi, H. Ma, Z. K. Wang, L. S. Liao, *Adv. Funct. Mater.* **2015**, *25*, 6671 – 6678; b) Y. Z. Xu, L. F. Zhu, J. J. Shi, X. Xu, J. Y. Xiao, J. Dong, H. J. Wu, Y. H. Luo, D. M. Li, Q. B. Meng, *ChemPhysChem* **2016**, *17*, 112 – 118.

[30] N. Adhikari, A. Dubey, E. A. Gaml, B. Vaagensmith, K. M. Reza, S. A. A. Mabrouk, S. P. Gu, J. T. Zai, X. F. Qian, Q. Q. Qiao, *Nanoscale* **2016**, *8*, 2693 – 2703.

[31] A. M. A. Leguy, Y. Hu, M. Campoy-Quiles, M. I. Alonso, O. J. Weber, P. Azarhoosh, M. van Schilfgaarde, M. T. Weller, T. Bein, J. Nelson, P. Docampo, P. R. F. Barnes, *Chem. Mater.* **2015**, *27*, 3397 – 3407.

[32] a) Z. Zhu, V. G. Hadjiev, Y. G. Rong, R. Guo, B. Cao, Z. J. Tang, F. Qin, Y. Li, Y. N. Wang, F. Hao, S. Venkatesan, W. Z. Li, S. Baldelli, A. M. Guloy, H. Fang, Y. D. Hu, Y. Yao, Z. M. Wang, J. M. Bao, *Chem. Mater.* **2016**, *28*, 7385 – 7393; b) C. Müller, T. Glaser, M. Plogmeyer, M. Sendner, S. Doring, A. A. Bakulin, C. Brzuska, R. Scheer, M. S. Pshenichnikov, W. Kowalsky, A. Pucci, R. Lovrincic, *Chem. Mater.* **2015**, *27*, 7835 – 7841.

[33] J. Gong, M. J. Yang, X. C. Ma, R. D. Schaller, G. Liu, L. P. Kong, Y. Yang, M. C. Beard, M. Lesslie, Y. Dai, B. B. Huang, K. Zhu, T. Xu, *J. Phys. Chem. Lett.* **2016**, *7*, 2879 – 2887.

[34] S. Ito, S. Tanaka, H. Nishino, *J. Phys. Chem. Lett.* **2015**, *6*, 881 – 886.

[35] a) M. B. Price, J. Butkus, T. C. Jellicoe, A. Sadhanala, A. Briane, J. E. Halpert, K. Broch, J. M. Hodgkiss, R. H. Friend, F. Deschler, *Nat. Commun.* **2015**, *6*, 8420; b) M. T. Trinh, X. X. Wu, D. Niesner, X. Y. Zhu, *J. Mater. Chem. A* **2015**, *3*, 9285 – 9290;c) L. Wang, C. McCleese, A. Kovalsky, Y. Zhao, C. Burda, *J. Am. Chem. Soc.* **2014**, *136*, 12205 – 12208.

[36] G. Grancini, V. D'Innocenzo, E. R. Dohner, N. Martino, A. R. S. Kandada, E. Mosconi, F. De Angelis, H. I. Karunadasa, E. T. Hoke, A. Petrozza, *Chem. Sci.* **2015**, *6*, 7305 – 7310.

[37] M. J. Li, S. Bhaumik, T. W. Goh, M. S. Kumar, N. Yantara, M. Gratzel, S. Mhaisalkar, N. Mathews, T. C. Sum, *Nat. Commun.* **2017**, *8*, 14350.

[38] J. J. Snellenburg, S. P. Laptenok, R. Seger, K. M. Mullen, I. H. M. van Stokkum, *J. Stat. Softw.* **2012**, *49*, 1 – 22.

Manuscript received: August 11, 2017
Accepted manuscript online: October 11, 2017
Version of record online: October 20, 2017